Temperature induced structural changes at interfaces and their influence on magnetic and electronic properties of ultrathin Fe/Al structures

2006 J. Phys.: Condens. Matter 18 1197

(http://iopscience.iop.org/0953-8984/18/4/008)

INSTITUTE OF PHYSICS PUBLISHING JOURNAL OF PHYSICS: CONDENSED MATTER

J. Phys.: Condens. Matter **18** (2006) 1197–1210 doi:10.1088/0953-8984/18/4/008

Temperature induced structural changes at interfaces and their influence on magnetic and electronic properties of ultrathin Fe/Al structures

R Brajpuriya[1], **A Sharma, S Tripathi, V R Reddy and S M Chaudhari**

University Grant Commission, Department of Atomic Energy, Consortium for Scientific Research, University Campus, Indore-452 017, India

E-mail: ranjeetbrajpuriya@yahoo.com

Received 8 October 2005
Published 9 January 2006
Online at stacks.iop.org/JPhysCM/18/1197

Abstract

Structural, magnetic and electronic properties of electron beam evaporated ultrathin Fe/Al structures are studied as a function of annealing temperature. The structural studies show that adjacent Fe and Al layers are partially intermixed during deposition, forming FeAl transition layers a few nanometres thick at the interfaces. However, at 200 °C, a large degree of atomic mixing causes a progressive loss of periodicity due to the formation of disordered intermetallic FeAl phase at the interfaces, which on further annealing at 400 °C transforms to Fe_3Al intermetallic phase. The magnetic and resistivity measurements show maximum coercivity, saturation field and resistivity values at 200 °C which then decrease above annealing temperatures. The corresponding valence band photoemission results show significant modifications in the Fe-3d as well as Al-3s density of states due to strong hybridization of sp–d states at the Fermi level. The observed magnetic and resistivity behaviour in each case is discussed and correlated with microstructural and electronic property changes due to the annealing treatment.

1. Introduction

The magnetic interactions between ferromagnetic films separated by non-magnetic metallic films have been a subject of extensive investigations from both the theoretical and experimental point of view. These kinds of artificial structures are expected to provide an understanding of surface magnetism and transport phenomena, such as interlayer magnetic-coupling, surface anisotropy, magneto-optical effect and giant magneto-resistance [1–3]. However, these interesting properties are greatly influenced by various microstructural multilayer (ML) parameters such as layer thickness, number of bilayers and the quality of interfaces formed

[1] Author to whom any correspondence should be addressed.

under different conditions [4, 5]. Up to now, much attention has been paid to the dependence of interlayer coupling on the spacer layer thickness and some studies have been carried out on micro-structural evolution and the changes of magnetic properties under thermal processing. Since multilayers are inherently metastable materials with nanometre-scale periodicity, the stability of the microstructure upon thermal annealing, particularly alloying and interdiffusion, critically alters the electronic and magnetic properties, which are sensitive to the evolution of microstructure [6–8]. Among various combinations of elements used to fabricate such multilayered film, much attention has been focused on the combination of elements having different crystal structure [9–11]. In this respect, the structure and phase composition of interfaces in multilayered binary Fe/Al system is of interest both from a fundamental point of view and with respect to questions concerning the reaction kinetics of an intermixing or phase formation after thermal treatment [12–14]. Fe/Al multilayer samples (MLSs) have also been studied extensively because of their attractive soft magnetic properties such as low coercivity and high saturation magnetization [15–17]. In addition to this, upon thermal treatment, they precipitate into various Fe–Al phases, which are important for high temperature structural applications and show excellent resistance to oxidation, sulfuration, and corrosion [14, 18].

In this paper, we report the effect of alloying on magnetic and electronic properties of ultrathin Fe/Al multilayers. The motivation for choosing this system was twofold. First, recently many interesting papers have been published dealing with the structural characterization of intermixing and phase formation in Fe/Al MLSs [19–22], but in all these cases the thickness of both Fe and Al layers are above 5 nm; and second, very few reports are available about the corresponding investigations of their magnetic, transport and electronic properties. Therefore, in order to gain basic understanding about micro-structural changes at much lower thicknesses ($\leqslant$2 nm) due to thermal annealing and their influence on the magnetic and electronic properties, we have prepared $[\mathrm{Fe}(2\ \mathrm{nm})/\mathrm{Al}(1\ \mathrm{nm})]_{x15}$ multilayers using an electron beam evaporation system [23] under ultrahigh vacuum (UHV) conditions and studied these properties as a function of annealing temperature.

2. Experimental procedure

$[\mathrm{Fe/Al}]_{x15}$ multilayers were deposited on float glass substrates by sequential evaporation of 2 nm Fe and 1 nm Al, under ultrahigh vacuum conditions at room temperature. Prior to deposition, *ex situ* cleaning of the substrates was done using the following chemical method. The glass substrates were initially washed with soap solution and rinsed with distilled water. After that they were kept in 5% chromic acid for 15 min, followed by washing with a continuous flow of distilled water. Before loading to the UHV chamber, they were dried using an infrared lamp. The base pressure inside the evaporation system was $\sim 2 \times 10^{-9}$ Torr, while during deposition it dropped to $\sim 1 \times 10^{-8}$ Torr. The deposition rate of 0.1 Å s^{-1} for both Fe and Al was maintained using a quartz crystal thickness monitor. A capping layer of 2.5 nm of Al was also deposited on top of the samples in order to protect the multilayers from oxidation. The first deposited layer on the substrate was of aluminium. To study the structural evolution upon thermal annealing and associated changes in magnetic and electronic properties, as-deposited films were subjected to thermal annealing in a furnace with a vacuum level better than 5×10^{-8} Torr in the temperature range 100–400 °C in an interval of 100 °C for 2 h.

For the determination of micro-structural changes in the MLSs upon annealing, grazing incidence x-ray diffraction (GIXRD) and reflectivity (GIXRR) measurements were carried out after each stage of annealing. All the GIXRD patterns are recorded at a 0.5° angle grazing incidence. These measurements were done using a Siemens D5000 diffractometer equipped with a sealed Cu tube as the source of x-rays with wavelength $\lambda = 1.542$ Å, operated at

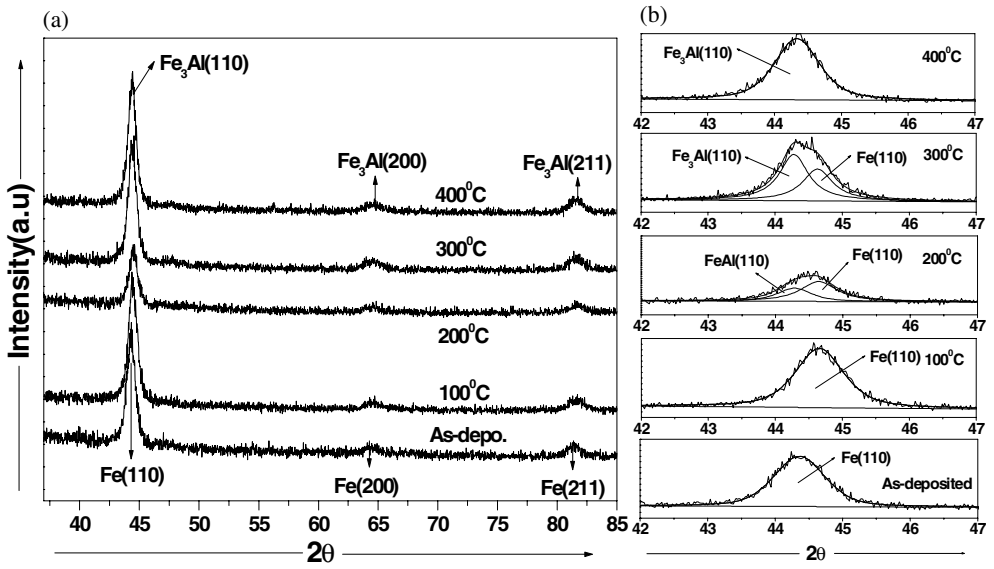

Figure 1. GIXRD patterns of (a) as-deposited as well as annealed Fe/Al MLSs and (b) fitted portion of the Fe (110) peak.

40 kV and 30 mA. AFM measurements were recorded using a DI Nanoscope-E AFM set up in contact mode. The associated changes in magnetic properties were characterized by means of the magneto optical Kerr effect (MOKE) technique with a laser source (He–Ne) of wavelength 632.8 nm. The corresponding transport properties were obtained by employing the four-probe resistivity method. An x-ray photoelectron spectroscopy (XPS) study was carried out using an OMICRON EA-125 photoelectron spectrometer at a base pressure better than 5×10^{-10} Torr. Mg Kα un-monochromatized radiation was employed for the analysis, with the source operated at an emission current of 10 mA and an anode voltage of 10 kV. A concentric hemispherical energy analyser (CHA) with 50 eV pass energy giving an overall resolution of $\sim$0.8 eV was used. Au $4f_{7/2}$ at 84.7 eV served as an external reference. Since the glass substrate is non-conducting, a charging effect was observed. To correct the shifts in binding energies of core levels due to the charging effect, the graphitic C 1s peak at 284.7 eV was used as an internal reference. The sample was sputtered with Ar^+ ions to clean the surface as well to reach the interface region before recording the VB photoemission spectra of the Fe/Al MLSs. This also provided the chemical composition of the film at different depths, averaged over the escape depth of photoelectrons ($\sim$4 nm). All the measurements reported in the present paper were carried out at room temperature.

3. Results and discussion

3.1. GIXRD measurements

Figure 1 show the GIXRD patterns of as-deposited as well as annealed Fe/Al MLSs. The diffraction pattern corresponding to an as-deposited sample displays three distinct crystalline peaks located at $2\theta = 44.32°$, 64.30° and 81.40°, and these are assigned to the reflections from α-Fe (110), Fe (200) and Fe (220) planes, respectively. The strong peak corresponding to Al (111) is expected at a 2θ value of 38.55°; however, we do not observe any reflections from Al

planes, indicating the amorphous nature of the deposited Al layer having 1 nm film thickness. The recorded XRD pattern also indicates the oriented growth of Fe layers mainly along the [110] direction. In addition to this, 2θ values corresponding to Fe reflections are also shifted towards lower 2θ values as compared to the bulk [24]. We interpret the shift in peak positions to be caused by the elongation of the interplanar distance d due to internal stresses in Fe layers induced by adjacent Al layers and their intermixing at the interfaces during deposition. Many researchers have also reported the occurrence of such an intermixing process during deposition in Fe/Al ML systems [6, 8, 19, 20]. However, in the case of the MLS annealed at 100 °C, all the peaks are shifted towards higher 2θ values (44.65°, 61.23°, 83.34°) and are attributed to the relaxation of stresses present in the as-deposited MLS. However, significant changes are observed in the GIXRD pattern, showing the structural transformation in the MLS annealed at 200 °C. The peaks become broad and simultaneously a reduction in peak intensity is also observed, as is clearly shown in figure 1(b) for peak Fe (110). These structural modifications in the MLS indicate the large degree of atomic mixing due to the diffusion of Al atoms into initially formed intermixed layer during deposition, leading to the formation of disordered FeAl phase at the interface. The Fe (110) peak can be fitted with two components: one at $2\theta = 44.3°$ corresponding to disordered FeAl intermetallic phase and the other at 44.64° corresponding to α-Fe. Further, the fitted GIXRD pattern of the MLS annealed at 300 °C shows increased intensity of the FeAl peak, suggesting the further growth of this phase at the interface. Finally, the MLS annealed at 400 °C, shows a clear peak only due to the FeAl phase at $2\theta = 44.39°$, indicating the complete transformation of the Fe/Al MLS to the FeAl phase. As suggested in a recent paper of Eggersmann *et al* on the diffusion in the intermetallic phases of the Fe–Al system, the mobility of Al atoms both in A2 and in B2 FeAl phases is higher than that of Fe atoms by at least a factor of 10 at 300 °C [25]. Therefore, it is expected that the highly mobile Al atoms would start diffusing into the relatively immobile lattice of Fe, leading to the formation of a disordered Fe–Al intermetallic layer at the interfaces. Further, their result indicates that after nucleation, the growth of intermetallic B2 phase mainly occurs through solid-state reaction of Al atoms at the B2/α-Fe interface. But, it is rather difficult to conclude from these measurements which phase will selectively form between the two existing phases of FeAl, namely, Fe_3Al (DO3) and FeAl (B2), since their 2θ values are almost overlapping. With respect to the B2 and DO3 phases, as indicated in the Fe-rich side of the Fe–Al phase diagram, the nucleation of the B2 phase is strongly favoured by thermodynamical forces, as their heats of formation are -25.1 (B2) and -15.7 (DO3) kJ mol^{-1}, respectively [26]. But the atomic densities of Fe and Al are 0.85×10^{23} and 0.6×10^{23} atoms cm^{-3} respectively, forming an average atomic concentration of Fe:Al = 3:1 in our case. Therefore, we conclude that in the present case non-stoichiometric Fe_3Al intermetallic phase was formed by annealing the sample at higher temperature.

3.2. GIXRR measurements

A better understanding of the inner structure of these multilayer samples can be attained by a careful analysis of the GIXRR results obtained after simulation of the MLS. Figure 2 shows the fitted GIXRR patterns of as-deposited as well as annealed Fe/Al MLSs. Different models were used to fit the experimental curves of figure 2, starting with a model of a $[Fe/FeAl/Fe]_{x15}$ trilayer stack with nominal composition (stage 1, figure 3) and ending with a model of complete intermixing (stage 3, figure 3). In order to determine the micro-structural parameters such as individual layer thickness, surface and interface roughness and intermixing at the interfaces, these experimentally measured GIXRR patterns were computer fitted using Parratt's formalism [27]. A summary of all parameters with best fit is given in table 1.

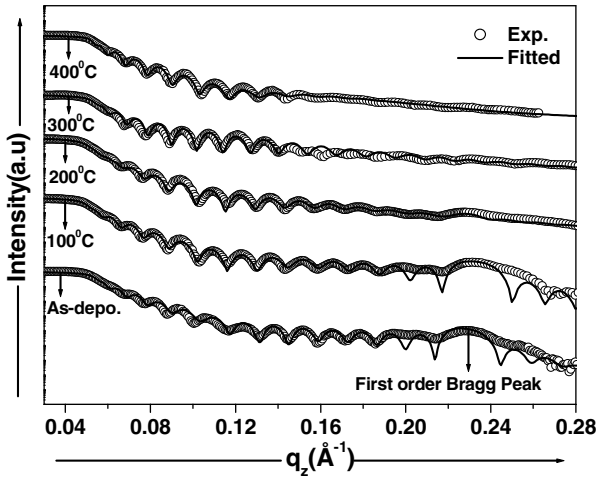

Figure 2. Fitted GIXRR patterns of as-deposited as well as annealed Fe/Al MLSs.

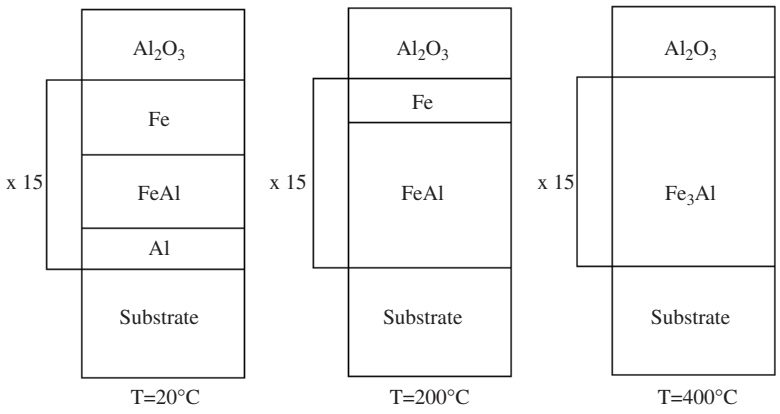

Figure 3. Proposed model for GIXRR patterns as a function of annealing temperature.

The GIXRR patterns recorded on the as-deposited sample as well as the sample annealed at 100 °C do not look like the typical patterns of a multilayer structure where one expects to find many oscillations due to both the structure and number of repetitions of the layers forming the period of the multilayer. The reason why this curve is different from the expected one can be immediately understood from the results reported in table 1. It is clearly seen from the fitted parameters that a relatively thick intermixed FeAl layer is formed at the Fe/Al interfaces in the case of the as-deposited (1.04 nm) MLS and the MLS annealed at 100 °C (1.23 nm), mainly accomplished by the diffusion of Al into Fe. Therefore, these results show that in the as-deposited sample, both Fe and Al layers start to intermix during deposition. One can easily understand that at these very small individual layer thicknesses, continuous layers are not expected. This effect causes a diffusion of interfaces between adjacent layers, which is responsible for the high values of surface roughness and observed reflectivity patterns.

The nature of the GIXRR pattern recorded on the MLS annealed at 200 °C is significantly different from the two cases previously discussed. In this case, the intensity of the first-order Bragg peak is reduced, reflecting the continuation of dissolution of the regular multilayer

Table 1. Parameters of individual layers of the multilayer determined by fitting a model to the experimental reflection curve. The curve obtained with the parameters is displayed in figure 2 (full line).

Layer	Compound	t (nm)	σ (nm)
Model 1, $T = 25\,^{\circ}$C			
5×1	Al_2O_3	2.618	0.961
4×15	Fe	1.503	1.092
3×15	FeAl	1.039	1.231
2×15	Al	0.279	0.519
1×1	Substrate	—	0.711
Model 2, $T = 100\,^{\circ}$C			
5×1	Al_2O_3	2.685	1.508
4×15	Fe	1.358	1.422
3×15	FeAl	1.238	1.093
2×15	Al	0.155	0.891
1×1	Substrate	—	0.702
Model 3, $T = 200\,^{\circ}$C			
4×1	Al_2O_3	2.653	1.739
3×15	Fe	0.741	0.441
2×15	FeAl	2.089	0.984
1×1	Substrate	—	1.012
Model 4, $T = 300\,^{\circ}$C			
4×1	Al_2O_3	2.827	0.312
3×15	Fe	0.212	0.786
2×15	Fe_3Al	2.549	1.023
1×1	Substrate	—	1.456
Model 5, $T = 400\,^{\circ}$C			
3×1	Al_2O_3	3.148	0.131
2×15	Fe_3Al	2.819	1.111
1×1	Substrate	—	1.784

structure. It can be seen from the fitted parameters (listed in table 1) that the thickness of the FeAl intermixed layer at the interface increased to 2.09 nm from 1.04 nm in the case of the as-deposited MLS. This substantial increase in thickness of the FeAl layer is a consequence of Al diffusion in the already formed FeAl intermixed layer during deposition. The fitted parameters also show complete consumption of the Al layer, showing transformation of the as-deposited (Fe–FeAl–Al) trilayer stack to a (Fe–FeAl) bilayer stack as shown in figure 3(b). As mentioned earlier, the GIXRD pattern recorded in this case also shows a substantial reduction in peak intensity due to the formation of disordered FeAl phase at the interface. However, the GIXRR patterns of MLSs annealed at 300 and 400 °C can be fitted with a single Fe_3Al layer having layer thicknesses 2.55 and 2.82 nm, respectively, suggesting the complete transformation of the Fe/Al MLSs to a single Fe_3Al layer. The corresponding transformation in the ML structure is shown schematically in figure 3(c).

3.3. AFM measurements

Further information about the structure and surface morphology can be obtained from AFM studies conducted on Fe/Al bilayer samples prepared under similar conditions to those for

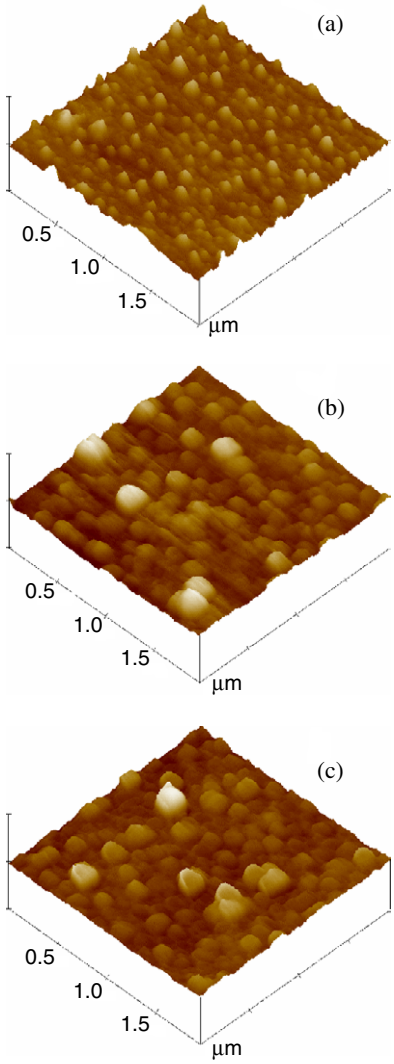

Figure 4. Three-dimensional AFM images of (a) as-deposited, (b) 200 °C and (c) 400 °C annealed Fe/Al bilayer samples.

(This figure is in colour only in the electronic version)

the multilayer samples. Figure 4 shows three-dimensional AFM images of (a) as-deposited, (b) 200 °C and (c) 400 °C annealed Fe/Al bilayer samples obtained from a $2 \times 2\ \mu m^2$ sample surface area using contact mode. It is clearly seen from figure 4(a) that in the as-deposited condition, the layers are not continuous and mainly show an island type growth, where Fe clusters are embedded in an Al matrix; yet a large free volume is available for the next Al layer, causing a very large surface roughness value of ∼1.734 nm. So one can easily understand the obtained reflectivity pattern in figure 2 by seeing in above AFM image why a well-defined multilayer structure is not observed in the case of the as-deposited MLS. After annealing at 200 °C, significant changes are observed in the surface morphology of the Fe/Al bilayer sample, as shown in figure 4(b). Both Fe and Al clusters are joined together to form

bigger clusters, resulting in large surface roughness value of ∼1.343 nm. However, a more continuous and flatter surface is obtained for the sample annealed at 400 °C as compared to above two cases, also in accordance with the previously discussed reflectivity pattern. The results obtained from the AFM study along with other structural investigations can help us in interpreting the observed resistivity and magnetization behaviour.

3.4. MOKE measurements

The MOKE measurements carried out on as-deposited as well as MLSs annealed at 100, 200, 300 and 400 °C are shown in figure 5. For all the measurements, the magnetic field was applied parallel to the surface of the films and hysteresis loops were recorded up to saturation magnetization. It can be seen that the M–H loop corresponding to the as-deposited multilayer film is square in shape, indicating that the distribution of anisotropy is rather sharp, which causes the domain magnetization switching beyond a certain applied magnetic field. The large vertical jumps with retentivity almost equal to saturation magnetization and lower coercivity value indicate the soft magnetic behaviour of the as-deposited sample with strong anisotropy leading to an in-plane easy direction of the magnetization. Similar M–H loop behaviour but with lower coercivity (H_c) value was obtained for the MLS annealed at 100 °C. These small changes in M–H loop behaviour at this temperature are mainly attributed to annealing of various point defects and release of stresses present in the as-deposited ML film. However, at 200 °C, we observed significant changes in the hysteresis loop behaviour. One can see that the shape of the square loop (as in the case of as-deposited film) changes to a smoother one, indicating a different type of interaction of domains and their wall motion with respect to applied magnetic field. A large increase in coercivity (23.86 Oe) and saturation field (101.34 Oe) has been observed at this temperature. In addition to this, the squareness ratio (M_r/M_s) decreases to a minimum (0.468), as shown in figure 6. Figure 6 shows the annealing temperature (T_a) dependence of coercivity (H_c), saturation field (H_s) and squareness ratio (M_r/M_s) of the film. The changes in observed magnetization behaviour at this temperature of annealing seem to be related to significant modifications in the microstructure of the as-deposited MLS. At this stage of annealing, as discussed earlier, GIXRD and GIXRR results clearly show substantial intermixing due to interdiffusion of Fe and Al, leading to the formation of a much thicker intermixed amorphous FeAl intermetallic layer at the interface. As a consequence, the as-deposited (Fe/FeAl/Al) multilayer structure has changed to an (Fe/FeAl) MLS. Therefore, observed changes in M–H loop can be attributed to the transformation of an (Fe/FeAl/Al) trilayer structure to an (Fe/FeAl) bilayer structure, which may alter the response of the applied magnetic field showing the gradual variation of domains with increased H_c, H_s and decreased M_r/M_s values. However, upon further annealing at higher temperatures, i.e. at 300 and 400 °C, the H_c and H_s values again reduce to 14.57 and 44.45 Oe with enhancement in the M_r/M_s ratio to 0.86. The difference in magnetization behaviour of the samples annealed at 300 and 400 °C from that annealed at 200 °C can be understood as follows.

In the FeAl alloy system, there exist mainly two ordered FeAl phases, namely Fe_3Al, having the DO3 structure and being ferromagnetic, and the FeAl phase, having the CsCl lattice structure and being non-magnetic in nature. These alloys are characterized by a direct ferromagnetic interaction between Fe–Fe sites and an anti-ferromagnetic super-exchange coupling between Fe sites mediated by Al atoms [28]. However, recent theoretical and experimental results reported by Reddy *et al* and Bogner *et al* suggest that the presence of any kind of disorder has a pronounced effect on the magnetic and transport properties of these alloys [29, 30]. In such alloys, it has been suggested that competing ferromagnetic and anti-ferromagnetic coupling is the deciding factor for inducing the magnetism. Therefore, from

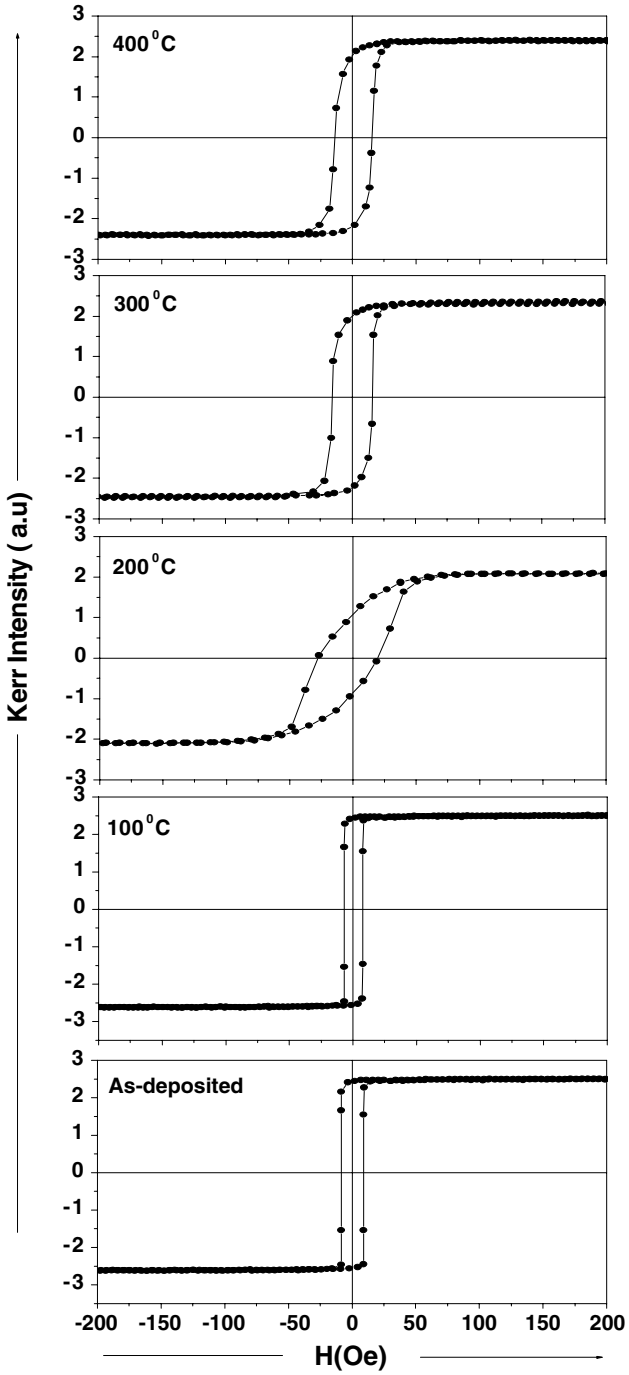

Figure 5. Hysteresis loops of as-deposited as well as annealed Fe/Al MLSs.

the above discussion it is most likely that the observed changes in magnetization behaviour at 200 °C are mainly due to the formation of disordered FeAl phase initially at the interface and its

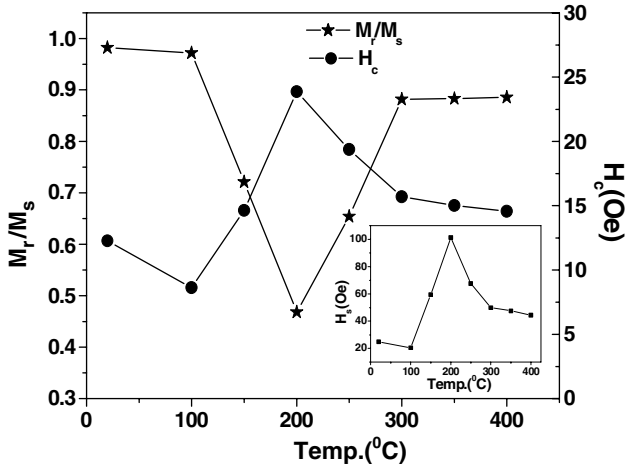

Figure 6. Annealing temperature dependence of in-plane coercivity, saturation field and squareness ratio.

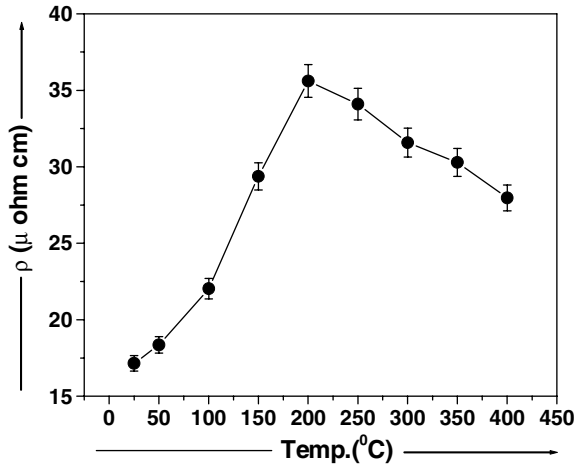

Figure 7. Variation of resistivity with temperature in Fe/Al MLSs.

subsequent growth converting it to Fe_3Al intermetallic phase at 400 °C, which is magnetically softer as compared to FeAl phase.

3.5. Resistivity measurements

The electrical resistivity of Fe/Al MLSs as a function of annealing temperature is shown in figure 7. The resistivity value for the as-deposited MLS is ∼17.14 $\mu\Omega$ cm, much higher than that of both its constituent elements. The reported resistivity values for pure bulk Fe and Al are 9.1 and 2.5 $\mu\Omega$ cm, respectively. The various factors such as intermixing at the interfaces, point defects and structural disorders present in as-deposited layers are mainly responsible for the high resistivity value in this case. From figure 7, one can further see that the resistivity increases sharply with temperature from 100 to 200 °C and shows a maximum value of 35.61 $\mu\Omega$ cm at 200 °C. However, the resistivity decreases upon further annealing the

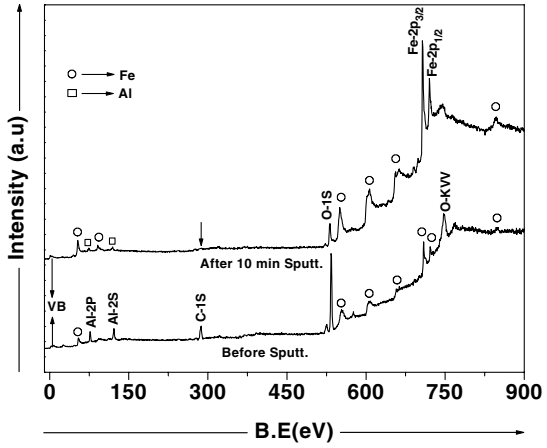

Figure 8. The survey scans of the as-deposited Fe/Al MLS recorded before and after sputtering.

MLS at higher temperatures, and shows a value of 27.96 $\mu\Omega$ cm at 400 °C. It is also reported that the resistivity value of the FeAl phase is higher than that of the Fe_3Al intermetallic phase. Therefore, the observed variations in resistivity behaviour as a function of annealing temperature can be understood as follows: (i) formation of a thin intermixed layer during deposition, (ii) Al migration into the initially formed intermixed region leading to the formation of disordered FeAl phase at the interface, and (iii) finally the formation and growth of Fe_3Al intermetallic phase at higher temperatures.

3.6. XPS measurements

In order to get more insight into the processes taking place at the surfaces and interfaces during annealing, we have also studied the thermal stability of the Fe/Al interface in the temperature range 100–400 °C using the XPS technique. For the sake of integrity of the discussion, the photoemission spectra shown in this section are all taken from the same multilayer sample.

Figure 8 show the survey scans of the as-deposited sample surface of the Fe/Al MLS before and after 10 min sputtering. From the spectrum (before sputtering) one can see that peaks corresponding to carbon (C), oxygen (O) and aluminium (Al) are clearly visible, whereas very small peaks due to iron (Fe) are observed. This presence of small Fe peaks is expected, as Fe is the second layer after the top Al (2.5 nm) capping layer. Since the sample was exposed to air, there are large quantities of absorbed C and O on the surface, as is evident from the spectrum. However, after sputtering the sample for 10 min, the intensity of C and O drops to a minimum with the appearance of buried Fe peaks at binding energy (BE) positions 706.8 eV (Fe-$2p_{3/2}$) and 719.8 eV (Fe-$2p_{1/2}$), indicating that the signals are coming from the first interface region. We also note that the reduction in the carbon content is more rapid than that of the oxygen content, and may be attributed to preferential sputtering of C with respect to reacted O. Hence the above results show that impurities were present only at the surface in the form of carbides and oxides in the Al layer and in elemental form in the Fe layer.

Figure 9 shows the valence band (VB) photoemission spectra of Fe/Al MLSs annealed (*in situ*) at (b) 200 °C and (c) 400 °C along with (a) 10 min sputtered as-deposited sample surface (for comparison), where the contribution from both Fe and Al are seen simultaneously from the first interface region. The VB spectrum corresponding to the as-deposited MLS shows three distinct features: a broad 3d photoemission band around 1.62 eV due to Fe below the

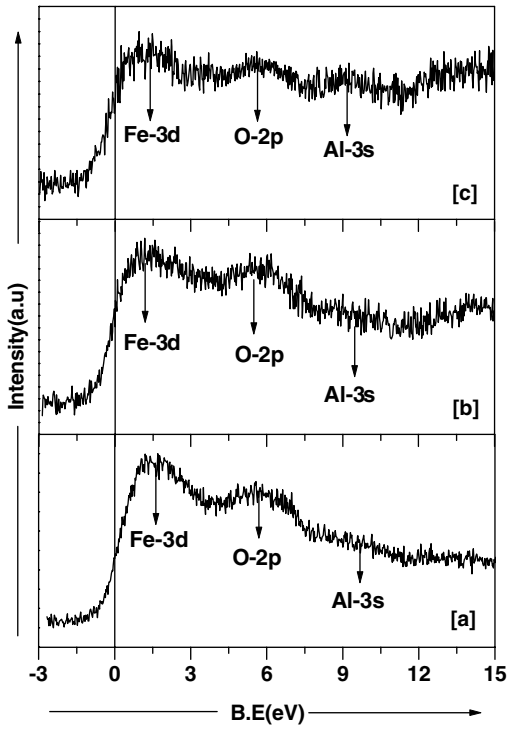

Figure 9. Valence band photoemission spectra of (a) as-deposited (b) 200 °C and (c) 400 °C annealed Fe/Al MLSs.

Fermi level and another two broad bands lying deeper in energy at 5.88 and 9.82 eV, which are attributed to π and σ molecular orbitals, respectively, formed by the hybridization of Al-3sp and O-2p orbitals [31] as shown in figure 9(a). The recorded spectrum in this case is mostly dominated by the photoemission band of Fe-3d. A sharp Fermi edge and a tail towards higher binding energies after the Fe-3d band corresponds to electron–hole pair excitations caused by the sudden creation of a photohole, and is a signature of metallic state of the sample. We note that these features are in excellent agreement with previous reports [32]. However, the VB spectrum recorded on the MLS annealed at 200 °C shows significant changes as compared to the as-deposited case. In this case, it is observed that the Fe-3d band is shifted by 0.24 eV towards lower binding energy (BE), i.e. towards the Fermi level, and becomes broad. In addition to this, it is also found that the total density of Fe-3d states is reduced to half as compared to the as-deposited case. Similarly, the VB photoemission spectrum corresponding to the 400 °C annealed Fe/Al MLS is shown in figure 8(c). In this case also it is found that the Fe-3d density of states is further modified and the emission band is further shifted by 0.12 eV towards the Fermi level. In addition to this, a clear appearance of the Al-3s band is also observed at 9.3 eV. All these changes suggest the strong hybridization of sp–d states at the Fermi level due to the charge transfer from valence Al-3p and Al-3s electrons to minority 3d orbitals of Fe, giving rise to FeAl intermetallic-like properties.

The above-mentioned changes in the magnetic, transport and valence band behaviour can be easily understood from the electronic structure of Fe and Al atoms. The outermost valence orbitals of Fe and Al atoms are ($3d^6 4s^2$) and ($3s^2 3p^1$), respectively. Due to the unfilled 3d orbitals of Fe, the orbitals are split into spin $\uparrow$ and spin $\downarrow$ states by an energy of 13.3 eV,

while for 4s orbitals it is small, i.e. 0.92 eV. A similar situation arises in the Al atom, as it contains only one unpaired electron and hence the spin splitting of the 3s and 3p orbitals is also small. The most important point is that the 3s orbitals of Al are very close in energy to the 3d orbitals of Fe, thus providing the grounds for a strong overlap between Fe-3d and Al-3s as these elements are alloyed. More interestingly, the 3p electrons of Al lie at an energy higher than the 3d and 4s electrons of Fe. Thus, as these elements are alloyed, one would expect a charge transfer from Al-3p to Fe-3d, as the 4s orbitals of Fe are full, as reflected in our valence band spectrum. This charge transfer would have an immediate effect on the resistivity as well as the magnetic moment of Fe due to filling of the 3d orbitals. Therefore, one expects to observe the changes in magnetization and resistivity behaviour with alloying.

4. Conclusion

We have studied the effect of FeAl phase formation on the magnetic, transport and electronic properties of electron beam evaporated ultrathin Fe/Al multilayer samples subjected to thermal annealing. The structural measurements show (a) formation of intermixed FeAl layers a few nanometres thick during deposition, (b) a large degree of atomic mixing due to the formation of disordered FeAl phase at 200 °C, and (c) finally a non-stoichiometric Fe_3Al phase at 400 °C. The observed changes in magnetic, transport and valence band behaviour are due to the strong hybridization of sp–d states near the Fermi level, giving rise to FeAl intermetallic-like properties.

Acknowledgments

The authors would like to thank Professor A Gupta for GIXRD and MOKE measurements. Special thanks are given for the help rendered by Mr S Potdar and Mr A Wadikar in depositing the multilayer samples. This work is dedicated to the memory of Dr S M Chaudhari who passed away untimely during this work.

References

[1] Baibich M N, Broto J M, Fert A, Nguyen F, Van Dau, Petroff F, Etienne P, Greeuzet G, Friederick A and Chazelas J 1988 *Phys. Rev. Lett.* **61** 2472
[2] Parkin S S P, Bhadra R and Roche K P 1991 *Phys. Rev. Lett.* **66** 2152
[3] Parkin S S P 1991 *Phys. Rev. Lett.* **67** 3598
[4] Allenspach R, Stampanoni M and Bischof A 1990 *Phys. Rev. Lett.* **65** 3344
[5] Lee C H, He H, Lamealas J, Vavra W, Uher C and Clarke R 1990 *Phys. Rev.* B **42** 1066
[6] Fonda E and Traverse A 2004 *J. Magn. Magn. Mater.* **268** 292
[7] Chaiken A, Michel R P and Wall M A 1996 *Phys. Rev.* B **53** 5518
[8] Chowdhury Ataur R and Freitag Andrea E 1996 *J. Appl. Phys.* **79** 6303
[9] Grimmer H, Böni P, Breirmeier U, Clemens D, Horisberger M, Mertins H C and Schäfers F 1998 *Thin Solid Films* **319** 73
[10] Tong L N, Pan M H, Wu J, Wu X S, Du J, Lu M, Feng D, Zhai H R and Xia H 1998 *Eur. Phys. J.* B **5** 61
[11] Gruenberg P, Schreiber R, Pang Y, Brodsky B M and Sower H 1986 *Phys. Rev. Lett.* **57** 2442
[12] Kattner U R 1990 *Binary Alloy Phase Diagrams* ed T B Massalski (Metals Park, OH: ASM International) p 147
[13] Bhattacharya P, Ishihara K N and Chattopadhyay K 2001 *Mater. Sci. Eng.* A **304** 250
[14] Deevi S C and Sikka V K 1996 *Intermetallics* **4** 357
[15] D'Orazio F, Gubbiotti G, Lucari F and Tassoni E 2002 *J. Magn. Magn. Mater.* **242** 535
[16] Chen H, Xu Q Y, Ni G, Lu J, Sang H, Zhang S Y and Du Y W 1999 *J. Appl. Phys.* **85** 5798
[17] Haeiwa T, Negoro H and Matsumoto M 1991 *J. Appl. Phys.* **69** 5346
[18] McKamey C G, DeVan J H, Tortorelli P F and Sikka V K 1991 *J. Mater. Res.* **6** 1779

[19] Checchetto R, Tosello C, Miotello A and Principi G 2001 *J. Phys.: Condens. Matter* **13** 811
[20] Mengucci P, Majni G, Di Cristoforo A, Checchetto R, Miotello A, Tosello C and Principi G 2003 *Thin Solid Films* **433** 205
[21] Levin A A, Meyer D C, Paufler P, Gorbunov A, Tselev A and Gawlitza P 2001 *J. Alloys Compounds* **320** 114
[22] Meyer D C, Richter K, Pauer P, Awlitza P and Holz T 2000 *J. Appl. Phys.* **87** 7218
[23] Chaudhari S M, Suresh N, Phase D M, Gupta A and Dasannacharya B A 1999 *J. Vac. Sci. Technol.* A **17** 242
[24] JCPDS file No 4-787 and 6-696
[25] Eggersmann M and Mehrer H 2000 *Phil. Mag.* **80** 1219
[26] Hultgren R, Desai P D, Hawkins D T, Gleiser M and Kelley K K 1973 *Selected Values of the Thermodynamic Properties of Binary Alloys* (Metals Park, OH: American Society for Metals) p 156
[27] Parratt L G 1954 *Phys. Rev.* **95** 359
[28] Sato H and Arrott A 1959 *Phys. Rev.* **114** 1427
[29] Reddy B V, Deevi S C, Reuse F A and Khanna S N 2001 *Phys. Rev.* B **64** 132408
[30] Bogner J *et al* 1998 *Phys. Rev.* B **58** 14992
[31] Thomas S and Sherwood P M A 1992 *Anal. Chem.* **64** 2488
[32] Paparazzo E, Dormann J L and Fiorani D 1983 *Phys. Rev.* B **28** 1154